

## Article

# Microstructural and Mechanical Behavior Investigations of Nb-Reinforced Mg–Sn–Al–Zn–Mn Matrix Magnesium Composites

Ali Ercetin <sup>1,\*</sup> , Özgür Özgün <sup>2</sup> , Kubilay Aslantaş <sup>3</sup> , Oguzhan Der <sup>4</sup> , Bekir Yalçın <sup>3</sup> , Ercan Şimşir <sup>5</sup>  and Muhammad Aamir <sup>6</sup> 

- <sup>1</sup> Department of Naval Architecture and Marine Engineering, Maritime Faculty, Bandırma Onyediy Eylül University, Bandırma 10200, Turkey
  - <sup>2</sup> Department of Occupational Health and Safety, Faculty of Health Sciences, Bingöl University, Bingöl 12000, Turkey; oozygun@bingol.edu.tr
  - <sup>3</sup> Department of Mechanical Engineering, Faculty of Technology, Afyon Kocatepe University, Afyonkarahisar 03200, Turkey; aslantas@aku.edu.tr (K.A.); bekiryalcin@aku.edu.tr (B.Y.)
  - <sup>4</sup> Department of Marine Vehicles Management Engineering, Maritime Faculty, Bandırma Onyediy Eylül University, Bandırma 10200, Turkey; oder@bandirma.edu.tr
  - <sup>5</sup> Department of Transportation Services, Sultandağı Vocational School, Afyon Kocatepe University, Afyonkarahisar 03900, Turkey; esimsir@aku.edu.tr
  - <sup>6</sup> School of Engineering, Edith Cowan University, Joondalup, WA 6027, Australia; m.aamir@ecu.edu.au
- \* Correspondence: aercetin@bandirma.edu.tr

**Abstract:** This research focuses on the fabrication and characterization of TAZ532-xNb composites, employing high-purity, micron-sized powders of Mg, Sn, Al, Zn, Mn, and Nb as the raw materials. These powders were subjected to a paraffin coating process aimed at mitigating oxidation. The formation of composites was achieved via hot pressing and was followed by surface preparation and analysis using scanning electron microscopy (SEM) and energy-dispersive spectroscopy (EDS). An X-ray diffraction (XRD) study was conducted to identify the microstructural phases. Quantitative assessments including the theoretical density, actual density, and relative density were computed, and their fluctuations in relation to the increasing Nb reinforcement ratio were scrutinized. Furthermore, the mechanical attributes of the composites, such as hardness and tensile strength, were assessed via experimental procedures. The absence of oxygen-related peaks in the XRD patterns endorsed the successful execution of the paraffin coating technique and protective gas atmosphere during sintering. The detection of  $\alpha$ -Mg, Mg<sub>2</sub>Sn, MgZn, Mg<sub>17</sub>Al<sub>12</sub>, and Nb phases within the Nb-reinforced composite patterns authenticated the formation of the intended phases. Notably, the relative density values of the composites surpassed 95%, indicating efficient sintering. SEM results disclosed a densely packed microstructure, with Nb reinforcement particles evenly distributed along the grain boundaries, devoid of particle clustering or significant grain growth. These composites manifested exceptional wetting characteristics, which can be attributed to the employment of Mg alloy as the matrix material. EDS data confirmed the proportions of Nb within the composites, aligning with the quantities incorporated during fabrication. The composites showcased an increase in microhardness values with the escalating Nb reinforcement ratio, credited to the harder constitution of Nb particles in comparison to the matrix alloy. Concurrently, tensile strength showed a significant improvement with the increment in Nb reinforcement, while elongation values peaked at a specific Nb reinforcement level. The positive evolution of tensile strength properties was ascribed to the escalated Nb reinforcement ratio, grain size, and consequent higher sample densities.

**Keywords:** magnesium matrix composite; Nb reinforcement; microstructure; tensile strength; hardness



**Citation:** Ercetin, A.; Özgün, Ö.; Aslantaş, K.; Der, O.; Yalçın, B.; Şimşir, E.; Aamir, M. Microstructural and Mechanical Behavior Investigations of Nb-Reinforced Mg–Sn–Al–Zn–Mn Matrix Magnesium Composites. *Metals* **2023**, *13*, 1097. <https://doi.org/10.3390/met13061097>

Academic Editor: Claudia Barile

Received: 29 May 2023

Revised: 6 June 2023

Accepted: 7 June 2023

Published: 10 June 2023



**Copyright:** © 2023 by the authors. Licensee MDPI, Basel, Switzerland. This article is an open access article distributed under the terms and conditions of the Creative Commons Attribution (CC BY) license (<https://creativecommons.org/licenses/by/4.0/>).

## 1. Introduction

One of the most significant challenges of the modern world is the increasing number of vehicles and the environmental impact they have [1]. Therefore, numerous solutions have been proposed to reduce fuel consumption and minimize the damage to the environment [2,3]. These solutions include reducing the weight of vehicles and promoting the use of lightweight alloys [4]. Magnesium (Mg), which is a lightweight metal, has drawn attention due to its property of being the lightest structural metal [5,6].

Pure Mg has a density of  $1.74 \text{ g/cm}^3$ , which is much lower than aluminum, titanium, zinc, and steel [5]. Despite being abundant in nature, the insufficient mechanical properties of pure Mg have led to the use of alloying elements for improved performance and engineering applications [7,8]. Common alloying elements include Al, Zn, Mn, and Sn, which can significantly affect the strength, hardness, elastic modulus, thermal conductivity, and corrosion resistance of Mg alloys [7,9].

The addition of Al to Mg forms the  $\beta$ - $\text{Mg}_{17}\text{Al}_{12}$  phase, which increases mechanical properties [10], but too much of it reduces the mechanical strength at high temperatures due to its high melting point [11,12]. Adding zinc improves mechanical properties and ductility while refining the microstructure [13,14]. The ductility of Mg-based materials increases with Zn content up to 2 wt.% but then decreases [15,16]. Sn forms the  $\text{Mg}_2\text{Sn}$  phase, which refines and pins grain boundaries [17,18]. As the melting temperature of  $\text{Mg}_2\text{Sn}$  is  $770.5 \text{ }^\circ\text{C}$ , the mechanical strength of Mg alloy is expected to improve with increased amounts of this phase [19,20].

The addition of various alloy elements to Mg has resulted in improvements in its hardness, strength, and ductility properties [21,22]. Although these improvements have made Mg alloys suitable for some applications, their strength and ductility properties are still insufficient for many other applications [23,24]. Hence, there is a growing need for the development of novel composite materials with superior properties that incorporate Mg alloy matrices [25].

Magnesium matrix composites (MgMCs) have high strength-to-weight ratio and are lighter in weight, which makes them an attractive alternative to traditional materials in many applications [26,27]. By adjusting the type, content, and size of the reinforcing phases and the processing methods used to manufacture them, the mechanical, thermal, and physical properties of magnesium composites can be customized [28,29]. These composites have been studied for their potential use in aerospace, automotive, biomedical, and sporting goods industries, among others [5,30].

MgMCs are materials composed of magnesium matrix reinforced with one or more secondary phases, typically ceramics or metals [31–33]. The addition of ceramic particles such as SiC,  $\text{Al}_2\text{O}_3$ , and TiC has been found to significantly improve the mechanical properties of magnesium matrix composites, such as strength, stiffness, and wear resistance [34–36]. However, there are important disadvantages of ceramic reinforcements [37]. One disadvantage of using ceramic reinforcement on magnesium matrix composites is the tendency for the ceramic particles to agglomerate during the fabrication process, which can result in nonuniform distribution and reduced mechanical properties [38,39]. Additionally, the difference in thermal expansion coefficients between the ceramic particles and the magnesium matrix can lead to thermal stress and cracking [33,40]. Finally, the high stiffness and brittleness of some ceramic materials can limit the ductility and toughness of the composite material [41,42].

Metal reinforcement, particularly with materials such as titanium, niobium, and nickel, offers several advantages in magnesium matrix composites [43,44]. Metal reinforcements can improve the overall processability of the composites [45,46], particularly during the fabrication stage, by providing better wettability, leading to more homogeneous microstructures and improved mechanical properties [33,47]. Nb is a promising reinforcement material for magnesium matrix composites due to its unique properties and zero-solubility in Mg [48,49]. Nb has a high melting point and thermal stability [50,51]. When added to magnesium, Nb can significantly improve the mechanical properties of the resulting

composite [52,53], such as increasing its strength and ductility. Additionally, Nb has a low density, which helps maintain the lightweight nature of magnesium composites [27,54]. Nb reinforcement can also improve the wear resistance, corrosion resistance, and high-temperature stability [55–57]. Furthermore, Nb has a good biocompatibility, which makes it an attractive reinforcement material for biomedical applications [58]. Overall, Nb reinforcement has several advantages for composites, making it a promising material for various engineering and biomedical applications [59,60].

One particular study by Vahid et al. [61] focused on producing magnesium-based composites with niobium particulates ranging from 5–15 wt.%. They utilized the disintegrated melt deposition technique, resulting in a uniform distribution of niobium particulates within the matrix without intermetallic compound formation. Microstructural analysis indicated refined grains and minimal porosity. Tensile testing demonstrated concurrent enhancements in hardness, 0.2% yield strength, and ultimate tensile strength with the addition of up to 10 wt.% Nb. However, exceeding 5 wt.% niobium in pure magnesium led to decreased ductility. Among the composites studied, the Mg/5 wt.% Nb composite exhibited the most favorable combination of strength and ductility, while the Mg/10 wt.% Nb composite displayed significant improvements in both strength and hardness compared to other composites.

Another study [62] investigated the effects of Nb addition to the Cu–Ni–Si–Mg alloy, focusing on mechanical properties, electrical conductivity, and microstructure. The results revealed that the alloy with 0.2 wt.% Nb exhibited superior overall characteristics after secondary aging, including increased hardness, tensile strength, breaking elongation, and electrical conductivity. Nb addition promoted the formation of smaller precipitates, specifically the  $\text{Ni}_2\text{Si}$  phase, and facilitated its transition from a coherent to an incoherent relationship with the matrix. Additionally, Nb increased the proportion of grain boundaries, facilitated the development of recrystallized texture and grains, and reduced the presence of cold-rolled texture and defects in the alloy.

The Powder Metallurgy (PM) technique is commonly used to produce composite materials as it allows for homogenous distribution of reinforcing elements, resulting in superior properties [25,63]. This involves mixing the matrix and reinforcement elements, compressing them in a metal mold, and sintering at a certain temperature in a protective gas atmosphere [64,65]. The relative density measurements of produced samples or pore ratio in the microstructure determine the success of the sintering process [66]. The hot-pressing method has been shown to yield higher relative density values compared to traditional PM methods [67,68]. However, when producing Mg matrix composites, it is crucial to prevent oxidation of Mg powders by coating them with paraffin and debinding them before the Hot Pressing (HP) process.

A novel method for producing high-performance composite samples has been developed by utilizing a hot-pressing technique and incorporating Nb particles into TAZ532 alloy matrix using high-purity and micron-sized metal powders, including Mg, Sn, Al, Zn, Mn, and Nb. The resulting composite samples exhibited high relative density values and were characterized by their microstructure and mechanical properties, demonstrating the potential of this approach for the development of advanced composite materials.

## 2. Materials and Methods

In this study, high-purity and micron-sized Mg, Sn, Al, Zn, Mn, Zn, Mn, and Nb powders were used to produce composites with TAZ532 alloy matrix containing Nb reinforcement at different ratios. Chemical compositions of TAZ532 matrix alloy are given in Table 1 and chemical compositions of Nb-reinforced composites are given in Table 2.

During the weighing and mixing of the powders, oxidation of Mg powders occurs as a result of contact with air. In order to prevent this situation, the paraffin coating technique was applied to Mg powders. Mg powders were obtained from Alfa Aesar company (Thermo Fisher (Kandel) GmbH, Deutschland, Germany) in 500 g vacuum packs. After weighing the gross weight of the package, it was opened in the glove box and Mg

powders were poured into the beaker containing hexane. The net weight of Mg powders was calculated by taking the difference between the (gross) weight of the package + Mg powder and the empty weight (tare) of the package. Precisia brand precision balance with a sensitivity of  $10^{-4}$  was used for weighing. Before opening the package in the glove box, the chamber was filled with high-purity argon gas and then vacuumed. The volume of Mg powders was calculated by the ratio of net weight to density and 20 vol. % paraffin was added to hexane+Mg powders in the beaker. In order to completely dissolve the paraffin in hexane, the beaker containing the mixture was placed in a sensitive heater and heated to 70 °C. While the beaker was on the heater, a propeller mixer was immersed into the mixture from the top. Stirring was continued at 180 rpm for 1 h until all the hexane was evaporated (Figure 1). The same stirring procedures were repeated for the preparation of the mixtures shown in Tables 1 and 2. Significant studies have been carried out on the effect of stirring speed, time, and sintering temperature on microstructural, mechanical, and corrosion properties [69–72]. Therefore, in this study, mixing speed, duration, and sintering parameters were obtained from experience in previous studies and optimum production parameters were applied [70,73].

**Table 1.** Chemical composition of TAZ532 alloy used as matrix.

Matrix Name	<45 $\mu\text{m}$ %99.8 Purity	<10 $\mu\text{m}$ %99.9 Purity	<10 $\mu\text{m}$ %99.9 Purity	<10 $\mu\text{m}$ %99.9 Purity	<10 $\mu\text{m}$ %99.9 Purity
	Mg (wt.%)	Sn (wt.%)	Al (wt.%)	Zn (wt.%)	Mn (wt.%)
TAZ532	89.85	5	3	2	0.15

**Table 2.** Chemical composition of TAZ532–xNb composite samples.

Sample Name	Composite Composition	<5 $\mu\text{m}$ %99.8 Purity	
		TAZ532 (wt.%)	Nb (wt.%)
Nb0	TAZ532 + %0 Nb	100	0
Nb1	TAZ532 + %1 Nb	99	1
Nb2	TAZ532 + %2 Nb	98	2
Nb4	TAZ532 + %4 Nb	96	4
Nb6	TAZ532 + %6 Nb	94	6

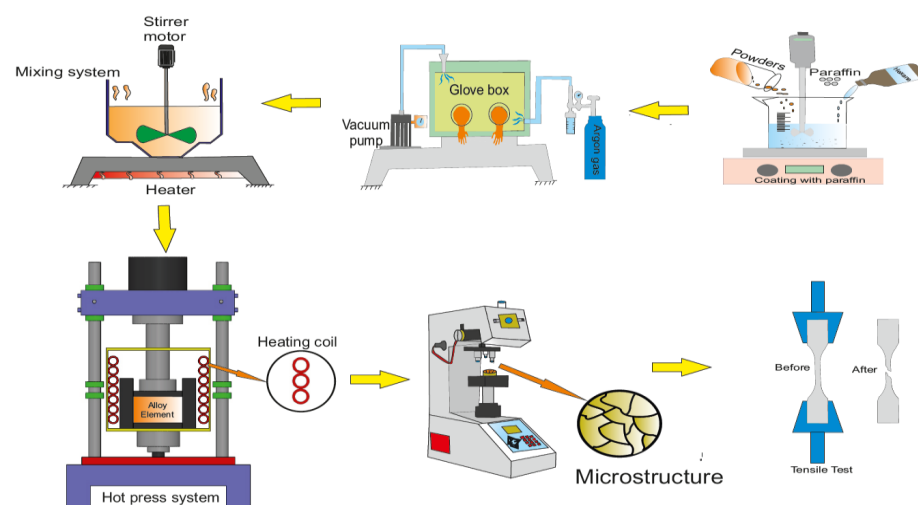


**Figure 1.** Schematic presentation of production, microstructural, and mechanical test of Nb-reinforced Mg matrix composites.

Samples of each mixture were produced on a hot press machine using a graphite molding system with dimensions of 30 mm length, 10 mm width, and 3.5 mm thickness (30 × 10 × 3.5 mm). After debonding at 300 °C for 30 min, sintering processes were carried out at 620 °C under 50 MPa pressure for 60 min using high-purity argon gas. The produced samples were sanded with 240, 400, 600, 800, 800, 1000, 1200, and 1500 grit sandpaper, followed by polishing and etching processes. The solution (5% nitric acid and 95% pure ethyl alcohol by volume), which is frequently used in the etching process of Mg-based materials, was used as a reference in the present study [74,75]. The etched samples were cleaned with distilled water and ethyl alcohol and then dried and made ready for SEM-EDS examinations.

The phases formed in the microstructure were determined by X-ray diffraction (XRD, Rigaku Ultima IV brand, Rigaku Corporation, Tokyo, Japan) analysis. Scanning electron microscopy (SEM, JEOL JSM 6510 brand, JEOL Ltd., Tokyo, Japan) and energy-dispersive spectroscopy (EDS, JEOL IXRF 550 brand, JEOL Ltd., Tokyo, Japan) analyses were applied for surface microstructure investigations. Theoretical density values were calculated according to Equation (1), measured density values were calculated according to Equation (2), and % relative density values were calculated according to Equation (3), which are used in accordance with ASTM B962-14 standard [76]. According to this standard, also known as the Archimedes principle, the specimens were first weighed in air and then weighed in distilled water [73,76].

$$\text{Theoretical density (g/cm}^3\text{)} = \frac{\text{Total Mass}}{\text{Total Volume}} = \frac{(\text{Mg mass}) + (\text{Sn mass}) + (\text{Zn mass})}{\left[\frac{\text{Mg mass}}{\text{Mg density}}\right] + \left[\frac{\text{Sn mass}}{\text{Sn density}}\right] + \left[\frac{\text{Zn mass}}{\text{Zn density}}\right]} \quad (1)$$

$$\text{Measured Density (g/cm}^3\text{)} = \frac{\text{Weight in air}}{(\text{Weight in air}) - (\text{Weight in water})} \text{ (Archimedes principle)} \quad (2)$$

$$\text{Relative Density (\%)} = \frac{\text{Actual Density}}{\text{Theoretical density}} \times 100 \quad (3)$$

Hardness and then tensile tests were applied to determine the mechanical properties of the samples. Prior to hardness measurement, each sample surface was subjected to precise sanding and polishing. Hardness tests were carried out using a Vickers hardness tester (Figure 1). Depending on the hardness of the sample, 200 g loads were applied for 10 s per sample. The average of the hardness values taken from 5 different areas of each sample was accepted as the average hardness value of the sample. MPIF-10 standard was used as the tensile specimen standard in the tensile tests of the specimens. Tensile tests were carried out in 3 repetitions for the specimens of each composition.

### 3. Results and Discussion

Figure 2 displays the X-ray diffraction (XRD) patterns of composite specimens that were fabricated by incorporating Nb reinforcements into a matrix alloy at various ratios. The XRD patterns reveal important information about the composition and structure of the samples. Notably, the absence of oxygen-related peaks in any of the specimens' patterns signifies the successful implementation of a paraffin coating and protective gas atmosphere during the sintering process. This protective environment prevents oxidation and ensures the integrity of the composite materials.

Analyzing the XRD patterns further, several peaks corresponding to different phases are observed consistently across all samples. These phases include  $\alpha$ -Mg, Mg<sub>2</sub>Sn, MgZn, and Mg<sub>17</sub>Al<sub>12</sub>. Interestingly, the intensities of these peaks remain similar across the various samples, indicating that there are no abnormal variations in the composition of the specimens. This uniformity in intensities suggests a consistent distribution of these phases within the composites. However, it is worth noting that peaks associated with the Nb phase are only present in the XRD patterns of specimens that contain Nb particle reinforcements.

As the ratio of Nb reinforcements increases, so does the intensity of the peaks related to the Nb phase. This trend implies a direct correlation between the amount of Nb added and the presence of the Nb phase in the composite materials. Indeed, it is often the case that the X-ray diffraction (XRD) peak intensities increase with higher concentrations of a given element. This is fundamentally because XRD peak intensity is directly related to the weight ratio of the phase within the material. Therefore, in the context of your observation, the XRD analysis shows the highest Nb peak intensities in the sample with a 6 wt.% Nb addition. This result suggests that there is a larger volume fraction of the Nb phase or Nb-related phases within this sample compared to those with lower Nb concentrations. These results align with expectations, given that a higher proportion of Nb is more likely to generate a higher volume fraction of Nb-based structures in the composite, thereby leading to more substantial XRD peak intensities.

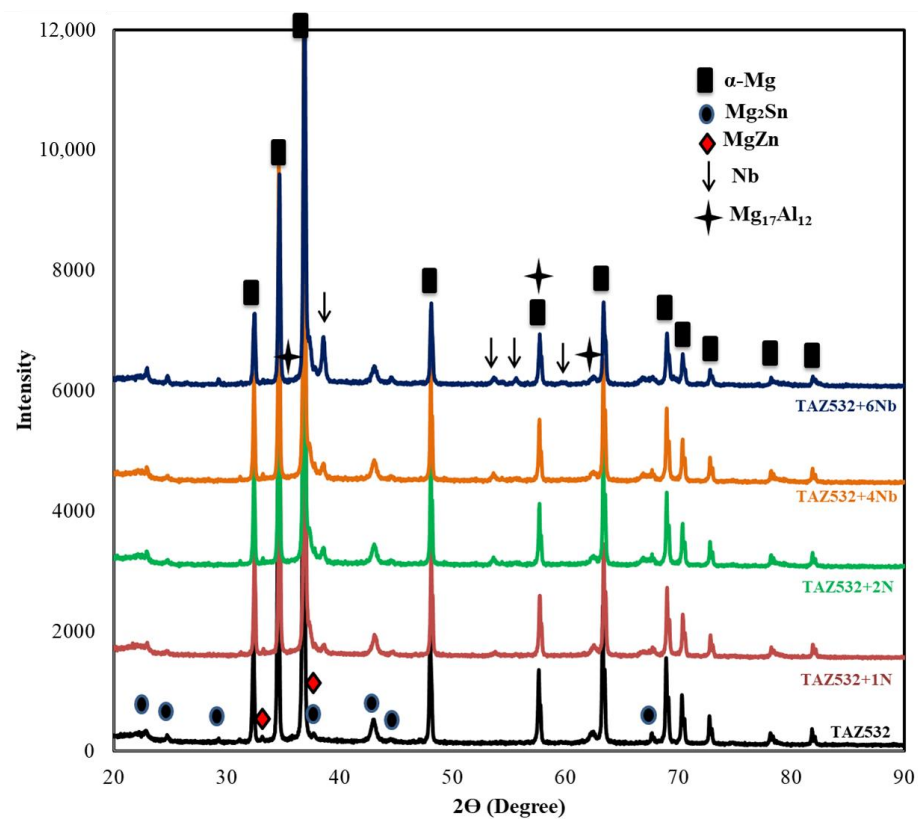


**Figure 2.** XRD patterns of Nb-particle-reinforced TAZ532 matrix composites.

Figure 3 illustrates the variations in theoretical density, measured density, and relative density data as the reinforcement ratio increases. The theoretical and measured real density values exhibit a consistent increase with the rising reinforcement ratio. This trend suggests that the incorporation of reinforcements contributes to a higher overall density of the composite specimens. However, the relative density values of samples containing a high level of reinforcement are lower compared to the other samples. Relative density refers to the ratio of the measured density to the theoretical density and serves as an indicator of how closely packed the particles are within the material. The lower relative density values in highly reinforced samples suggest that achieving a denser packing of particles becomes more challenging as the reinforcement content increases. Literature studies frequently indicate that a relative density value exceeding 95% for materials produced through powder metallurgy signifies the successful implementation of the sintering process [77,78]. Interestingly, in the present study, the relative density value of the TAZ532 matrix alloy surpasses 99%. Even the lowest relative density value among the Nb-reinforced samples, which amounts to 98.05%, exceeds the aforementioned 95% threshold mentioned in the

literature. This outcome indicates the successful production of TAZ532–xNb composite samples using the hot-pressing method. Therefore, it is expected that the microstructure of these composites will exhibit a significantly low pore fraction, emphasizing the dense and compact nature of the materials.

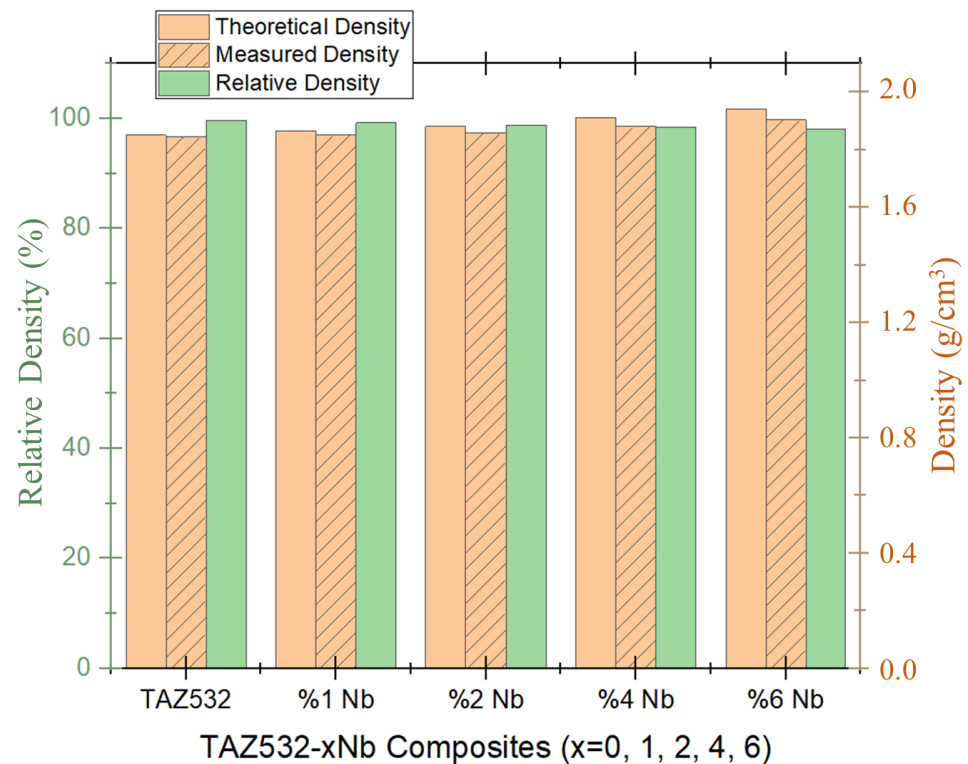


**Figure 3.** Theoretical, measured, and % relative density values of TAZ532–xNb composite samples.

The SEM images of TAZ532–xNb composites are presented in Figure 4, showcasing the surface morphology of the samples. Upon careful examination of these images, it becomes evident that the samples exhibit a highly dense microstructure. Grains and grain boundaries can be clearly observed, indicating the crystalline structure of the material. Notably, the microstructure appears devoid of any visible pore structures, indicating a lack of voids within the material. The microstructure images presented in Figure 4 further corroborate the information provided by the relative density graphs in Figure 3. The SEM images reveal that the Nb reinforcement particles are uniformly distributed along the grain boundaries of the material. Significantly, there is no evidence of particle clustering in any specific region. This uniform distribution of the reinforcement particles suggests an effective dispersion process during the fabrication of the composites. Both the present study and previous literature research [75,79,80] have demonstrated that the production method, specifically the P/M method employed, plays a crucial role in achieving a homogeneous microstructure. The amount of Nb particles at the grain boundaries increases with higher reinforcement ratios, indicating a proportional relationship between the reinforcement level and particle density.

Interestingly, even with an elevated density of Nb particles at the grain boundaries, our observations reveal an absence of grain growth within the microstructure. This phenomenon can be correlated with the role of reinforcing particles which act as effective barriers, effectively inhibiting the expansion of individual grains. The presence of hard reinforcement structures homogeneously distributed along the grain boundaries prevents grain growth, as supported by similar results in the literature [75,76,81]. The uniform distribution of these hard structures effectively impedes the movement and coalescence of adjacent grains, resulting in a constrained microstructure with limited grain growth. The

average grain sizes of the composite samples containing 0%, 1%, 2%, 4%, and 6% by weight of Nb, respectively, were obtained as 17.10  $\mu\text{m}$ , 12.21  $\mu\text{m}$ , 10.26  $\mu\text{m}$ , 9.89  $\mu\text{m}$ , and 8.08  $\mu\text{m}$ , respectively.

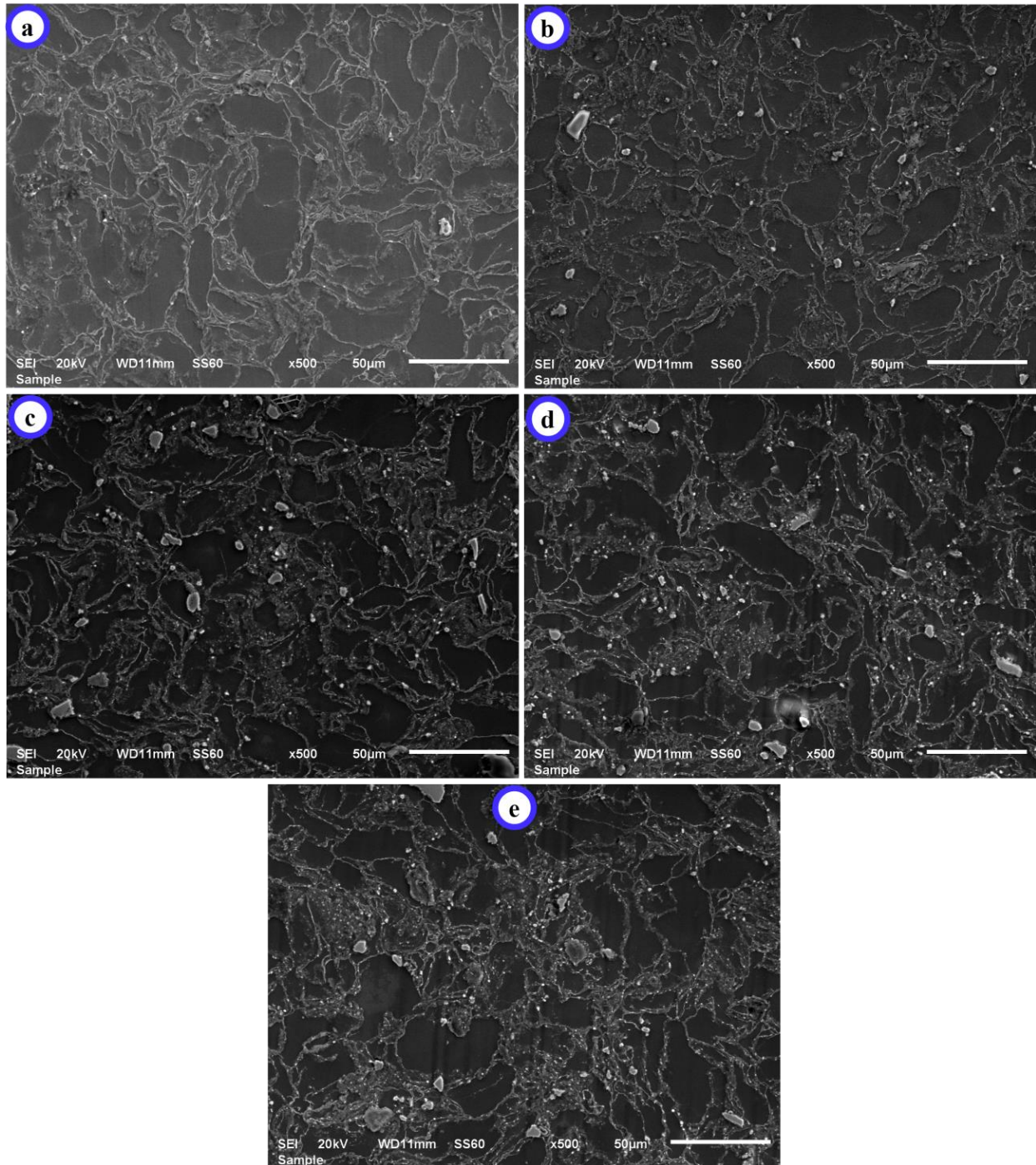


**Figure 4.** SEM images of TAZ532–xNb composite samples: (a) TAZ532 matrix, (b) 1 wt.% Nb-reinforced, (c) 2 wt.% Nb-reinforced, (d) 4 wt.% Nb-reinforced, (e) 6 wt.% Nb-reinforced.

Another notable observation derived from the SEM images is the achievement of complete wetting at a high level in all samples. The phenomenon of wetting refers to the ability of a liquid or molten phase to uniformly spread and adhere to the solid surface of another material. In the case of the TAZ532–xNb composites, the SEM images reveal that the reinforcing particles and the matrix material exhibit excellent wetting behavior,

indicating strong interfacial bonding. The use of a magnesium (Mg) alloy as the matrix material contributes significantly to the high wetting properties observed in the samples. Magnesium alloys are known for their favorable wetting characteristics when combined with other materials. In a separate study conducted by Suresh et al. [82], it was specifically found that Mg enhances the wetting behavior of composite materials. This suggests that the presence of the Mg alloy in the TAZ532-xNb composites contributes to the establishment of a favorable interfacial interaction between the matrix and the reinforcement. Complete wetting in the TAZ532-xNb composites indicates that the molten magnesium alloy has effectively spread and covered the surface of the reinforcing particles during the manufacturing process. This complete coverage facilitates intimate contact between the matrix and the reinforcement, resulting in a strong interfacial bond and improved load transfer between the phases. The enhanced wetting properties contribute to the overall mechanical performance of the composites, including improved strength, stiffness, and durability.

The SEM image, taken at  $\times 1000$  magnification, of the TAZ532 matrix composite containing 2 wt.% Nb by weight is provided in Figure 5. Concentrated at the grain boundaries, intermetallic phases and reinforcement particles such as niobium (Nb) serve to bolster the material's structure, playing a pivotal role in improving its mechanical properties. In our previous knowledge [6,15,73,75], the  $\alpha$ -Mg structure is conspicuously situated within the intergranular regions, often discerned via its distinctive black to dark gray pigmentation, an identifier designated as (mark 1) for clarity and communication efficiency. Transitioning to the structural elements labeled as (mark 2), these are present directly on the grain boundary. These formations exhibit a striking, white coloration and are laden with a high concentration of both Mg and Sn. Upon rigorous evaluation using X-ray diffraction (XRD) analytical methods, these particular structures have been definitively categorized as belonging to the  $Mg_2Sn$  phase, a compound of particular interest. Advancing to the (mark 3) designation, this involves a structure that distinctly resides on the grain boundary and is conspicuous by its uninterrupted, linear form. It bears a dark gray color, indicative of its composition. This structure is found to be rich in Mg and Al, hence aligning it with the  $Mg_{17}Al_{12}$  phase. This phase is a critical component of Mg-Al-based alloys, which are lauded for their superior mechanical properties and broad utility in numerous structural applications. The structures of mark 4 significantly contrasted on the grain boundaries are distinguished by both large and small geometric formations that bear a stark, white coloration. Composed primarily of niobium (Nb) particles, they reflect the inherent characteristics of this transition metal, notable for its high melting point and superior mechanical properties.

Figure 6 showcases the results of energy-dispersive X-ray spectroscopy (EDS) analysis conducted on the surface of TAZ532-xNb composite samples. The EDS analysis was performed using the same SEM images presented in Figure 4, allowing for a comprehensive investigation of the elemental composition and distribution within the samples. In Figure 6A, the EDS results for the TAZ532 matrix alloy are presented. These results demonstrate a close correspondence between the obtained ratios of elements and the ratios of elements added during the sample production process. The elemental composition determined by the EDS analysis aligns well with the expected composition, indicating the accuracy and reliability of the analysis technique. Furthermore, as the content of Nb particle reinforcement increases in the TAZ532-xNb composites, there is a corresponding increase in the Nb ratios obtained from the EDS analysis (Figure 6B-E). This trend is illustrated in Figure 6B, where the Nb ratios are observed to progressively rise with higher levels of reinforcement. Importantly, the EDS results closely match the added ratios of Nb during the production of the composite samples. The consistency between the added ratios and the EDS results suggests that the fabrication process effectively incorporates the desired proportions of reinforcement particles into the composite material. The EDS analysis confirms that the Nb particles are present in the expected quantities, which is crucial for achieving the desired mechanical properties and performance of the composites. By utilizing the SEM images for EDS analysis, it becomes possible to obtain spatially resolved elemental infor-

mation. This enables researchers to assess the distribution of different elements within the composite samples, gaining insights into the homogeneity and uniformity of the material.

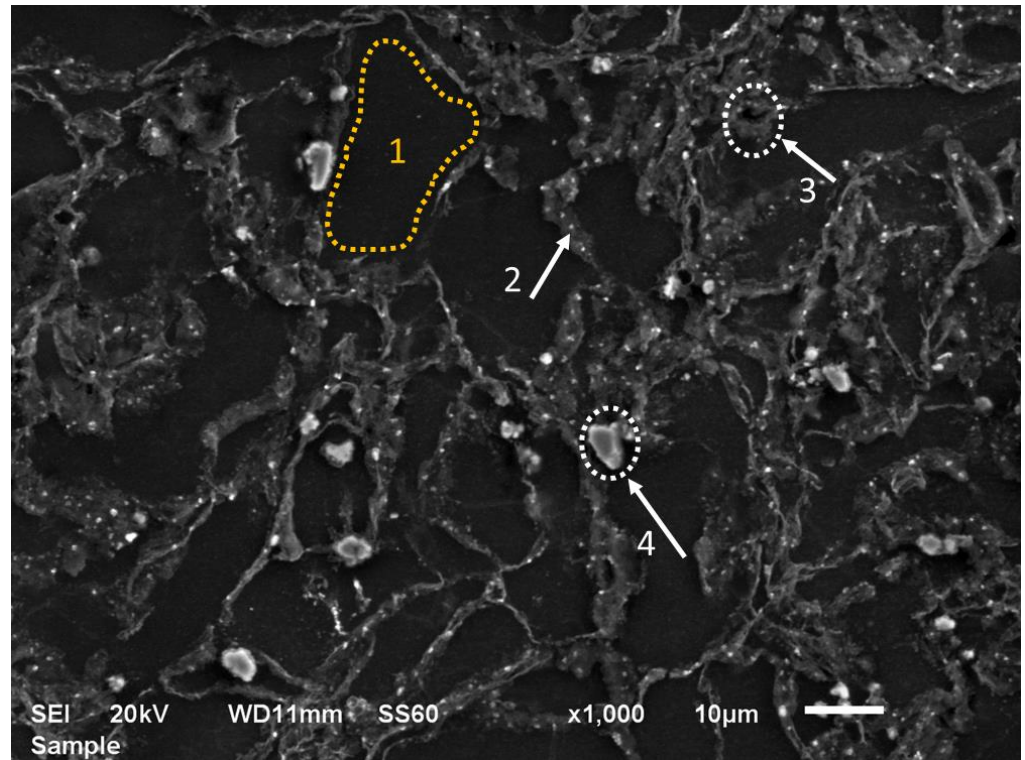
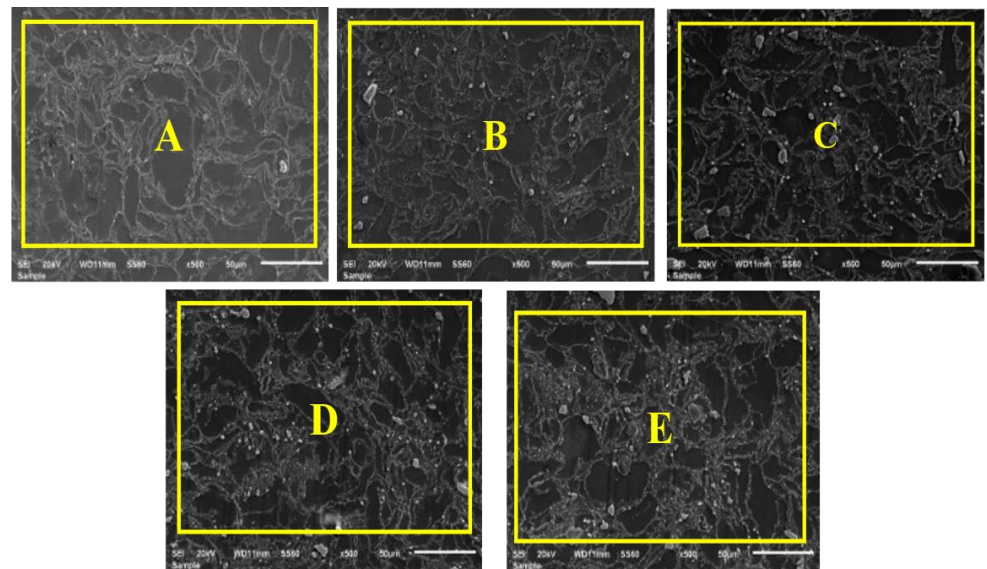


Figure 5. SEM image (1000× magnification) of 2 wt.% Nb-reinforced TAZ532 matrix composite.



A			B			C			D			E		
Elt.	Conc	Units												
Mg	90.526	wt. %	Mg	90.333	wt. %	Mg	89.831	wt. %	Mg	87.895	wt. %	Mg	86.018	wt. %
Al	2.853	wt. %	Al	1.984	wt. %	Al	2.001	wt. %	Al	1.892	wt. %	Al	2.007	wt. %
Mn	0.188	wt. %	Mn	0.123	wt. %	Mn	0.127	wt. %	Mn	0.155	wt. %	Mn	0.179	wt. %
Zn	1.725	wt. %	Zn	1.013	wt. %	Zn	1.113	wt. %	Zn	1.046	wt. %	Zn	1.015	wt. %
Sn	4.708	wt. %	Nb	1.159	wt. %	Nb	2.239	wt. %	Nb	3.746	wt. %	Nb	5.711	wt. %
	100.000	wt. %	Sn	5.388	wt. %	Sn	4.689	wt. %	Sn	5.267	wt. %	Sn	5.070	wt. %
				100.000	wt. %									

Figure 6. Areal EDS results of TAZ532–xNb composite samples: (A) TAZ532 matrix, (B) 1 wt.% Nb-reinforced, (C) 2 wt.% Nb-reinforced, (D) 4 wt.% Nb-reinforced, (E) 6 wt.% Nb-reinforced.

The microhardness values of the TAZ532–xNb composite samples are presented in Figure 7, providing insights into the mechanical properties of the composites. The average microhardness values for the composite samples, which contain different weight ratios of Nb reinforcement (0 wt.%, 1 wt.%, 2 wt.%, 4 wt.%, and 6 wt.%) within the TAZ532 matrix alloy, were determined as 73.3, 76.5, 79.2, 83.0, and 88.1 HV, respectively.

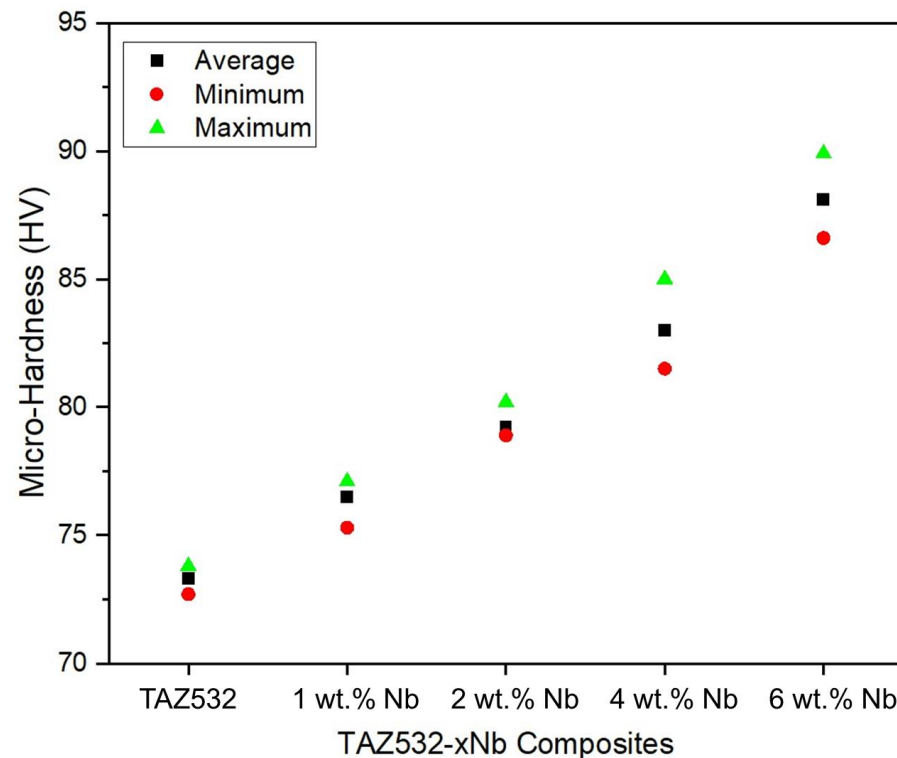


**Figure 7.** Microhardness values of TAZ532–xNb composite samples.

A noticeable trend is observed in the results, where the microhardness values consistently increase with the addition of Nb at different weight ratios. This suggests that the Nb reinforcement particles play a significant role in enhancing the hardness of the composites. The observed increase in microhardness values can be attributed to the inherent hardness of the Nb particles, which possess a harder structure compared to the alloy matrix.

When Nb particles are incorporated into the TAZ532 matrix alloy, they act as reinforcing agents that strengthen the material. The presence of these harder particles creates additional barriers to dislocation motion and deformation within the material. As a result, the resistance to plastic deformation and the overall hardness of the composites are enhanced.

The continuous increase in microhardness values with increasing Nb weight ratios indicates that the strengthening effect becomes more prominent as the reinforcement content rises. The higher the Nb content in the composites, the greater the number of reinforcing particles present, leading to a higher density of hard barriers within the matrix. This increased density of Nb particles effectively hinders dislocation movement and provides more resistance to plastic deformation, resulting in higher microhardness values.

The observed relationship between the Nb content and microhardness values confirms the reinforcing role of the Nb particles in improving the mechanical properties of the TAZ532–xNb composites. The incorporation of Nb reinforcement contributes to the increased hardness, which is an essential characteristic for applications where enhanced strength is desired.

The strength and elongation values obtained from the tensile testing of the TAZ532–xNb composite samples are presented in Figure 8, providing important insights into their mechanical behavior. The tensile strength values corresponding to different weight ratios

of Nb reinforcement (0 wt.%, 1 wt.%, 2 wt.%, 4 wt.%, and 6 wt.%) within the TAZ532 matrix alloy were determined as 101.01, 120.18, 138.48, 183.29, and 211.75 MPa, respectively.

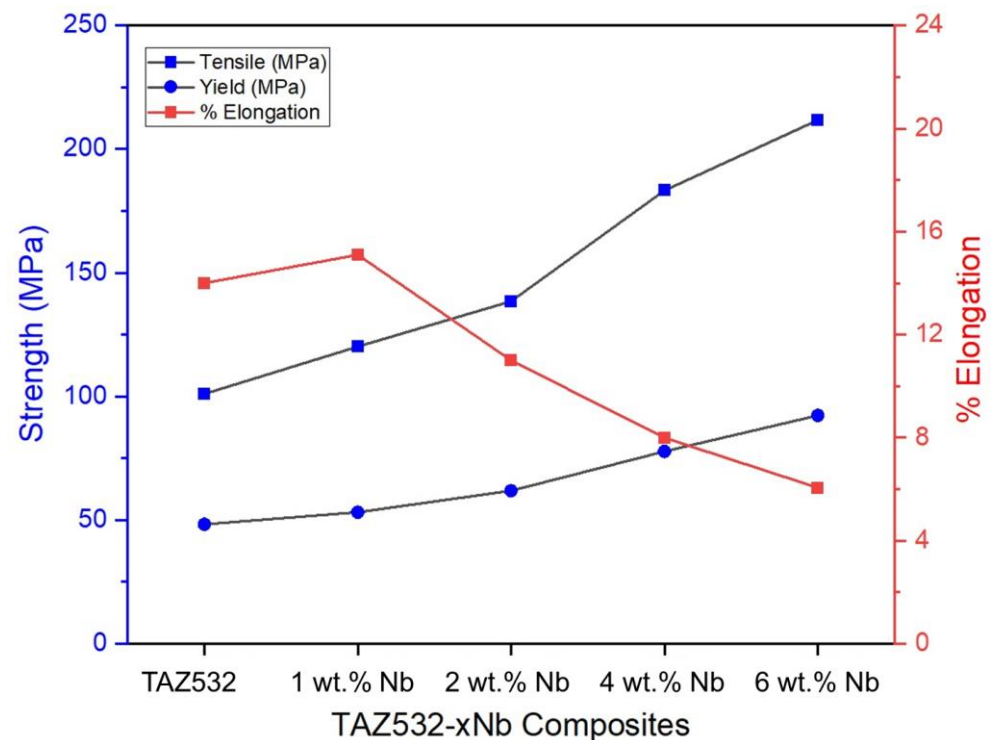


**Figure 8.** Yield strength, tensile strength, and % elongation values of TAZ532-xNb composite specimens.

A clear trend is observed in the results, indicating that the tensile strength properties are significantly improved with increasing Nb addition. As the Nb weight ratio increases, there is a corresponding enhancement in both the yield strength and tensile strength of the composites. This suggests that the Nb reinforcement plays a crucial role in reinforcing the material and enhancing its mechanical strength.

Furthermore, the elongation values of the composites also exhibit an interesting behavior. Initially, as the Nb reinforcement level increases, the elongation values tend to increase, indicating improved ductility. However, beyond a certain Nb reinforcement level, the elongation values may begin to plateau or even decrease. This observation suggests that, while the Nb reinforcement enhances strength, there may be a trade-off with the material's ductility beyond a certain threshold.

The increased Nb reinforcement ratio in the composites contributes to the positive development of the tensile strength properties. The reinforcing particles, which possess a higher strength compared to the matrix alloy, effectively hinder dislocation movement and promote load transfer within the material during tensile loading [78].

Moreover, the increase in Nb reinforcement ratio also leads to increased sample densities. The higher density of the composites, achieved through the incorporation of Nb particles, plays a significant role in enhancing the tensile strength properties. The increased density contributes to improved interfacial bonding between the matrix and reinforcement, resulting in effective load transfer and resistance to deformation [83].

#### 4. Conclusions

This manuscript presents a study on the fabrication and characterization of TAZ532-xNb composites, where high-purity and micron-sized powders of Mg, Sn, Al, Zn, Mn, and Nb were used to produce composites with a TAZ532 alloy matrix containing Nb reinforcement at different ratios. The paraffin coating technique was successfully employed

to prevent the oxidation of Mg powders during weighing and mixing. The mixing speed, duration, and sintering parameters were determined based on previous studies to achieve optimum production parameters.

- The X-ray diffraction (XRD) analysis confirmed the presence of  $\alpha$ -Mg,  $Mg_2Sn$ , and  $Mg_{17}Al_{12}$  phases in all composite samples, while the Nb phase was observed only in specimens with Nb reinforcement. The intensity of Nb-related peaks increased with higher Nb reinforcement ratios, reaching the highest values in samples with a weight ratio of 6 wt.% Nb addition.
- Theoretical and measured density values showed an increasing trend with an increasing reinforcement ratio. The relative density values of the composite samples exceeded the 95% threshold, indicating successful sintering. Scanning electron microscopy (SEM) images revealed a highly dense microstructure without any pore structures. The Nb reinforcement particles were uniformly distributed along the grain boundaries, effectively preventing grain growth. Complete wetting between the matrix alloy and Nb particles was achieved, attributed to the use of Mg alloy as the matrix.
- Energy-dispersive spectroscopy (EDS) analysis confirmed the presence of Nb in the composite samples, with the obtained ratios closely matching the added ratios during production. The microhardness values increased with the addition of Nb reinforcement, as the harder Nb particles contributed to the overall hardness of the composites.
- Tensile testing showed that the tensile strength values improved significantly with increasing Nb addition, while the elongation values increased up to a certain Nb reinforcement level. The increased Nb reinforcement ratio and sample densities played a crucial role in enhancing the tensile strength properties.

The results indicate successful production of TAZ532-xNb composite samples with a homogeneous microstructure, high wetting properties, and improved mechanical properties. These conclusions contribute to the understanding of the fabrication and performance of Nb-reinforced composites, highlighting their potential for various engineering applications. It is believed that an important contribution has been made to the scientific community. Additionally, Mg-based composites can offer lighter device usage options for cell phone and computer users. Furthermore, it has been demonstrated in this study that the P/M method is applicable to the manufacturing of Mg-based new composite materials, thus contributing to scientific research in this aspect.

**Author Contributions:** Conceptualization, A.E., Ö.Ö., K.A., O.D., B.Y. and E.Ş.; methodology, A.E., Ö.Ö., K.A. and O.D.; validation, A.E., Ö.Ö., K.A., O.D., B.Y. and E.Ş.; formal analysis, A.E., Ö.Ö., K.A., O.D., B.Y. and E.Ş.; investigation, A.E., Ö.Ö., K.A., O.D., B.Y. and E.Ş.; resources, A.E., Ö.Ö. and K.A.; data curation, A.E., Ö.Ö., K.A., O.D., B.Y. and E.Ş.; writing—original draft preparation, A.E., Ö.Ö., K.A., O.D., B.Y., E.Ş. and M.A.; writing—review and editing, A.E., Ö.Ö., K.A., O.D., B.Y., E.Ş. and M.A.; visualization, A.E., O.D. and E.Ş.; project administration, A.E.; funding acquisition, A.E., O.D. and M.A. All authors have read and agreed to the published version of the manuscript.

**Funding:** This study is founded by Bingöl University Scientific Research Projects Coordination Unit of Turkey (BÜBAP) with BAP-MMF-2020.00.002 project number.

**Data Availability Statement:** Not applicable.

**Acknowledgments:** Authors thank Bingöl University Scientific Research Projects Coordination Unit of Turkey (BÜBAP) and Bingol University for providing production process and microstructural investigations. The authors also thank Afyon Kocatepe University for providing the tensile tests.

**Conflicts of Interest:** The authors declare no conflict of interest.

## References

1. Li, Z.; Khajepour, A.; Song, J. A Comprehensive Review of the Key Technologies for Pure Electric Vehicles. *Energy* **2019**, *182*, 824–839. [[CrossRef](#)]
2. Borowski, P. Digitization, Digital Twins, Blockchain, and Industry 4.0 as Elements of Management Process in Enterprises in the Energy Sector. *Energies* **2021**, *14*, 1885. [[CrossRef](#)]
3. Tran, M.-K.; Akinsanya, M.; Panchal, S.; Fraser, R.; Fowler, M. Design of a Hybrid Electric Vehicle Powertrain for Performance Optimization Considering Various Powertrain Components and Configurations. *Vehicles* **2020**, *3*, 20–32. [[CrossRef](#)]
4. Alfattani, R.; Yunus, M.; Mohamed, A.F.; Alamro, T.; Hassan, M.K. Assessment of the Corrosion Behavior of Friction-Stir-Welded Dissimilar Aluminum Alloys. *Materials* **2021**, *15*, 260. [[CrossRef](#)] [[PubMed](#)]
5. Abazari, S.; Shamsipur, A.; Bakhsheshi-Rad, H.R.; Ismail, A.F.; Sharif, S.; Razzaghi, M.; Ramakrishna, S.; Berto, F. Carbon Nanotubes (CNTs)-Reinforced Magnesium-Based Matrix Composites: A Comprehensive Review. *Materials* **2020**, *13*, 4421. [[CrossRef](#)]
6. Ercetin, A. A Novel Mg-Sn-Zn-Al-Mn Magnesium Alloy with Superior Corrosion Properties. *Metall. Res. Technol.* **2021**, *118*, 504. [[CrossRef](#)]
7. Sharma, S.K.; Saxena, K.K.; Malik, V.; Mohammed, K.A.; Prakash, C.; Buddhi, D.; Dixit, S. Significance of Alloying Elements on the Mechanical Characteristics of Mg-Based Materials for Biomedical Applications. *Crystals* **2022**, *12*, 1138. [[CrossRef](#)]
8. Prasad, S.V.S.; Prasad, S.B.; Verma, K.; Mishra, R.K.; Kumar, V.; Singh, S. The Role and Significance of Magnesium in Modern Day Research—A Review. *J. Magnes. Alloy.* **2022**, *10*, 1–61. [[CrossRef](#)]
9. Radha, R.; Sreekanth, D. Insight of Magnesium Alloys and Composites for Orthopedic Implant Applications—A Review. *J. Magnes. Alloy.* **2017**, *5*, 286–312. [[CrossRef](#)]
10. Korgiopoulos, K.; Langelier, B.; Pegguleryuz, M. Mg<sub>17</sub>Al<sub>12</sub> Phase Refinement and the Improved Mechanical Performance of Mg–6Al Alloy with Trace Erbium Addition. *Mater. Sci. Eng. A* **2021**, *812*, 141075. [[CrossRef](#)]
11. Liu, S.; Guo, H. Influence of Heat Treatment on Microstructure and Mechanical Properties of AZ61 Magnesium Alloy Prepared by Selective Laser Melting (SLM). *Materials* **2022**, *15*, 7067. [[CrossRef](#)]
12. Zhou, P.; Wang, H.; Nie, H.; Cheng, W.; Niu, X.; Wang, Z.; Liang, W. Effect of ECAP Temperature on Precipitation and Strengthening Mechanisms of Mg–9Al–1Si Alloys. *J. Mater. Res.* **2018**, *33*, 1822–1829. [[CrossRef](#)]
13. Razzaghi, M.; Mirzadeh, H.; Emamy, M. Unraveling the Effects of Zn Addition and Hot Extrusion Process on the Microstructure and Mechanical Properties of As-Cast Mg–2Al Magnesium Alloy. *Vacuum* **2019**, *167*, 214–222. [[CrossRef](#)]
14. El Mahallawy, N.; Ahmed Diaa, A.; Akdesir, M.; Palkowski, H. Effect of Zn Addition on the Microstructure and Mechanical Properties of Cast, Rolled and Extruded Mg–6Sn–XZn Alloys. *Mater. Sci. Eng. A* **2017**, *680*, 47–53. [[CrossRef](#)]
15. Ercetin, A. Application of the Hot Press Method to Produce New Mg Alloys: Characterization, Mechanical Properties, and Effect of Al Addition. *J. Mater. Eng. Perform.* **2021**, *30*, 4254–4262. [[CrossRef](#)]
16. Lei, B.; Dong, Z.; Yang, Y.; Jiang, B.; Yuan, M.; Yang, H.; Wang, Q.; Huang, G.; Song, J.; Zhang, D.; et al. Influence of Zn on the Microstructure and Mechanical Properties of Mg–Gd–Zr Alloy. *Mater. Sci. Eng. A* **2022**, *843*, 143136. [[CrossRef](#)]
17. Akkoyun, F.; Ercetin, A. Automated Grain Counting for the Microstructure of Mg Alloys Using an Image Processing Method. *J. Mater. Eng. Perform.* **2022**, *31*, 2870–2877. [[CrossRef](#)]
18. Zhao, Z.Y.; Guan, R.G.; Shen, Y.F.; Bai, P.K. Grain Refinement Mechanism of Mg–3Sn–1Mn–1La Alloy during Accumulative Hot Rolling. *J. Mater. Sci. Technol.* **2021**, *91*, 251–261. [[CrossRef](#)]
19. Zhou, J.; Jafari Nodooshan, H.; Li, D.; Zeng, X.; Ding, W. Microstructure and Tensile Properties of the Mg–6Zn–4Al–XSn Die Cast Magnesium Alloy. *Metals* **2019**, *9*, 113. [[CrossRef](#)]
20. Mo, N.; Tan, Q.; Birmingham, M.; Huang, Y.; Dieringa, H.; Hort, N.; Zhang, M.-X. Current Development of Creep-Resistant Magnesium Cast Alloys: A Review. *Mater. Des.* **2018**, *155*, 422–442. [[CrossRef](#)]
21. Sezer, N.; Evis, Z.; Koç, M. Additive Manufacturing of Biodegradable Magnesium Implants and Scaffolds: Review of the Recent Advances and Research Trends. *J. Magnes. Alloy.* **2021**, *9*, 392–415. [[CrossRef](#)]
22. Alateyah, A.I.; Aljohani, T.A.; Alawad, M.O.; El-Hafez, H.A.; Almutairi, A.N.; Alharbi, E.S.; Alhamada, R.; El-Garaihy, B.W.; El-Garaihy, W.H. Improved Corrosion Behavior of AZ31 Alloy through ECAP Processing. *Metals* **2021**, *11*, 363. [[CrossRef](#)]
23. Song, J.; She, J.; Chen, D.; Pan, F. Latest Research Advances on Magnesium and Magnesium Alloys Worldwide. *J. Magnes. Alloy.* **2020**, *8*, 1–41. [[CrossRef](#)]
24. Fakhar, N.; Sabbaghian, M. A Good Combination of Ductility, Strength, and Corrosion Resistance of Fine-Grained ZK60 Magnesium Alloy Produced by Repeated Upsetting Process for Biodegradable Applications. *J. Alloys Compd.* **2021**, *862*, 158334. [[CrossRef](#)]
25. Mussatto, A.; Ahad, I.U.; Mousavian, R.T.; Delaure, Y.; Brabazon, D. Advanced Production Routes for Metal Matrix Composites. *Eng. Rep.* **2021**, *3*. [[CrossRef](#)]
26. Haghshenas, M. Mechanical Characteristics of Biodegradable Magnesium Matrix Composites: A Review. *J. Magnes. Alloy.* **2017**, *5*, 189–201. [[CrossRef](#)]
27. Dieringa, H. Processing of Magnesium-Based Metal Matrix Nanocomposites by Ultrasound-Assisted Particle Dispersion: A Review. *Metals* **2018**, *8*, 431. [[CrossRef](#)]
28. Zhou, M.Y.; Ren, L.B.; Fan, L.L.; Zhang, Y.W.X.; Lu, T.H.; Quan, G.F.; Gupta, M. Progress in Research on Hybrid Metal Matrix Composites. *J. Alloys Compd.* **2020**, *838*, 155274. [[CrossRef](#)]

29. Singh, L.; Singh, B.; Saxena, K.K. Manufacturing Techniques for Metal Matrix Composites (MMC): An Overview. *Adv. Mater. Process. Technol.* **2020**, *6*, 441–457. [[CrossRef](#)]
30. Tan, J.; Ramakrishna, S. Applications of Magnesium and Its Alloys: A Review. *Appl. Sci.* **2021**, *11*, 6861. [[CrossRef](#)]
31. Dinaharan, I.; Zhang, S.; Chen, G.; Shi, Q. Titanium Particulate Reinforced AZ31 Magnesium Matrix Composites with Improved Ductility Prepared Using Friction Stir Processing. *Mater. Sci. Eng. A* **2020**, *772*, 138793. [[CrossRef](#)]
32. Sardar, S.; Karmakar, S.K.; Das, D. Ultrasonic Assisted Fabrication of Magnesium Matrix Composites: A Review. *Mater. Today Proc.* **2017**, *4*, 3280–3289. [[CrossRef](#)]
33. Yang, H.; Chen, X.; Huang, G.; Song, J.; She, J.; Tan, J.; Zheng, K.; Jin, Y.; Jiang, B.; Pan, F. Microstructures and Mechanical Properties of Titanium-Reinforced Magnesium Matrix Composites: Review and Perspective. *J. Magnes. Alloy.* **2022**, *10*, 2311–2333. [[CrossRef](#)]
34. Arokiasamy, S.; Anand Ronald, B. Experimental Investigations on the Enhancement of Mechanical Properties of Magnesium-Based Hybrid Metal Matrix Composites through Friction Stir Processing. *Int. J. Adv. Manuf. Technol.* **2017**, *93*, 493–503. [[CrossRef](#)]
35. Karthick, E.; Mathai, J.; Michael Tony, J.; Marikkannan, S.K. Processing, Microstructure and Mechanical Properties of Al<sub>2</sub>O<sub>3</sub> and SiC Reinforced Magnesium Metal Matrix Hybrid Composites. *Mater. Today Proc.* **2017**, *4*, 6750–6756. [[CrossRef](#)]
36. Balasubramanian, I.; Maheswaran, R.; Manikandan, V.; Patil, N.; Raja, M.A.; Singari, R.M. Mechanical Characterization and Machining of Squeeze Cast AZ91D/SiC Magnesium Based Metal Matrix Composites. *Procedia Manuf.* **2018**, *20*, 97–105. [[CrossRef](#)]
37. Omanović-Miklićanin, E.; Badnjević, A.; Kazlagić, A.; Hajlovac, M. Nanocomposites: A Brief Review. *Health Technol.* **2020**, *10*, 51–59. [[CrossRef](#)]
38. Kasaeian-Naeini, M.; Sedighi, M.; Hashemi, R.; Delavar, H. Microstructure, Mechanical Properties and Fracture Toughness of ECAPed Magnesium Matrix Composite Reinforced with Hydroxyapatite Ceramic Particulates for Bioabsorbable Implants. *Ceram. Int.* **2023**, *49*, 17074–17090. [[CrossRef](#)]
39. Qin, Y.; Tian, Y.; Peng, Y.; Luo, L.; Zan, X.; Xu, Q.; Wu, Y. Research Status and Development Trend of Preparation Technology of Ceramic Particle Dispersion Strengthened Copper-Matrix Composites. *J. Alloys Compd.* **2020**, *848*, 156475. [[CrossRef](#)]
40. Wang, X.; Wang, X.; Hu, X.; Wu, K. Effects of Hot Extrusion on Microstructure and Mechanical Properties of Mg Matrix Composite Reinforced with Deformable TC4 Particles. *J. Magnes. Alloy.* **2020**, *8*, 421–430. [[CrossRef](#)]
41. Mirmohammadi, S.A.; Pasini, D.; Barthelat, F. Modeling, Design and Tailoring of a Tough, Strong and Stiff Multilayered Bone Graft Material. *J. Mech. Behav. Biomed. Mater.* **2022**, *134*, 105369. [[CrossRef](#)] [[PubMed](#)]
42. Clancy, A.J.; Anthony, D.B.; De Luca, F. Metal Mimics: Lightweight, Strong, and Tough Nanocomposites and Nanomaterial Assemblies. *ACS Appl. Mater. Interfaces* **2020**, *12*, 15955–15975. [[CrossRef](#)] [[PubMed](#)]
43. Behera, M.P.; Dougherty, T.; Singamneni, S. Conventional and Additive Manufacturing with Metal Matrix Composites: A Perspective. *Procedia Manuf.* **2019**, *30*, 159–166. [[CrossRef](#)]
44. Sankhla, A.; Patel, K.M. Metal Matrix Composites Fabricated by Stir Casting Process—A Review. *Adv. Mater. Process. Technol.* **2022**, *8*, 1270–1291. [[CrossRef](#)]
45. Kumar, V.M.; Venkatesh, C.V. A Comprehensive Review on Material Selection, Processing, Characterization and Applications of Aluminium Metal Matrix Composites. *Mater. Res. Express* **2019**, *6*, 072001. [[CrossRef](#)]
46. Naseer, A.; Ahmad, F.; Aslam, M.; Guan, B.H.; Harun, W.S.W.; Muhamad, N.; Raza, M.R.; German, R.M. A Review of Processing Techniques for Graphene-Reinforced Metal Matrix Composites. *Mater. Manuf. Process.* **2019**, *34*, 957–985. [[CrossRef](#)]
47. Torabi Parizi, M.; Habibolahzadeh, A.; Ebrahimi, G.R. Optimizing and Investigating Influence of Manufacturing Techniques on the Microstructure and Mechanical Properties of AZ80-0.5Ca-1.5Al<sub>2</sub>O<sub>3</sub> Nanocomposite. *Mater. Chem. Phys.* **2017**, *199*, 485–496. [[CrossRef](#)]
48. Shanthi, M.; Jayaramanavar, P.; Vyas, V.; Seenivasan, D.V.S.; Gupta, M. Effect of Niobium Particulate Addition on the Microstructure and Mechanical Properties of Pure Magnesium. *J. Alloys Compd.* **2012**, *513*, 202–207. [[CrossRef](#)]
49. Jayalakshmi, S.; Sahu, S.; Sankaranarayanan, S.; Gupta, S.; Gupta, M. Development of Novel Mg–Ni<sub>60</sub>Nb<sub>40</sub> Amorphous Particle Reinforced Composites with Enhanced Hardness and Compressive Response. *Mater. Des.* **2014**, *53*, 849–855. [[CrossRef](#)]
50. Serrano-Ruiz, J.C.; Luque, R.; Sepúlveda-Escribano, A. Transformations of Biomass-Derived Platform Molecules: From High Added-Value Chemicals to Fuels via Aqueous-Phase Processing. *Chem. Soc. Rev.* **2011**, *40*, 5266. [[CrossRef](#)]
51. Pathak, S.; Velisavljevic, N.; Baldwin, J.K.; Jain, M.; Zheng, S.; Mara, N.A.; Beyerlein, I.J. Strong, Ductile, and Thermally Stable Bcc-Mg Nanolaminates. *Sci. Rep.* **2017**, *7*, 8264. [[CrossRef](#)]
52. Ceschini, L.; Dahle, A.; Gupta, M.; Jarfors, A.E.W.; Jayalakshmi, S.; Morri, A.; Rotundo, F.; Toschi, S.; Singh, R.A. *Aluminum and Magnesium Metal Matrix Nanocomposites*; Springer: Singapore, 2017; ISBN 978-981-10-2680-5.
53. Ali, M.; Hussein, M.A.; Al-Aqeeli, N. Magnesium-Based Composites and Alloys for Medical Applications: A Review of Mechanical and Corrosion Properties. *J. Alloys Compd.* **2019**, *792*, 1162–1190. [[CrossRef](#)]
54. Kumar, D.; Phanden, R.K.; Thakur, L. A Review on Environment Friendly and Lightweight Magnesium-Based Metal Matrix Composites and Alloys. *Mater. Today Proc.* **2021**, *38*, 359–364. [[CrossRef](#)]
55. Yufan, S.; Hanguang, F.; Xuelong, P.; Shuting, S.; Jian, L.; Yongping, L. Effect of Process Parameters and Niobium Carbide Addition on Microstructure and Wear Resistance of Laser Cladding Nickel-based Alloy Coatings. *Materwiss Werkstofftech* **2020**, *51*, 54–65. [[CrossRef](#)]

56. Eze, A.A.; Jamiru, T.; Sadiku, E.R.; Durowoju, M.O.; Kupolati, W.K.; Ibrahim, I.D. Considering the Use of Niobium and Titanium to Enhance Electrical and Mechanical Properties of Copper at Higher Operational Temperature Application. *SN Appl. Sci.* **2019**, *1*, 74. [[CrossRef](#)]
57. Castillejo, F.E.; Marulanda, D.M.; Olaya, J.J.; Alfonso, J.E. Wear and Corrosion Resistance of Niobium–Chromium Carbide Coatings on AISI D2 Produced through TRD. *Surf. Coat. Technol.* **2014**, *254*, 104–111. [[CrossRef](#)]
58. Olivares-Navarrete, R.; Olaya, J.J.; Ramírez, C.; Rodil, S.E. Biocompatibility of Niobium Coatings. *Coatings* **2011**, *1*, 72–87. [[CrossRef](#)]
59. Acchar, W.; Segadães, A.M. Properties of Sintered Alumina Reinforced with Niobium Carbide. *Int. J. Refract. Met. Hard Mater.* **2009**, *27*, 427–430. [[CrossRef](#)]
60. Zhu, L.; Ren, X.; Wang, X.; Kang, X.; Zheng, R.; Feng, P. Microstructure and High-Temperature Oxidation Resistance of MoSi<sub>2</sub>-ZrO<sub>2</sub> Composite Coatings for Niobium Substrate. *J. Eur. Ceram. Soc.* **2021**, *41*, 1197–1210. [[CrossRef](#)]
61. Vahid, A.; Hodgson, P.; Li, Y. Reinforced Magnesium Composites by Metallic Particles for Biomedical Applications. *Mater. Sci. Eng. A* **2017**, *685*, 349–357. [[CrossRef](#)]
62. Wang, W.; Wang, J.; Li, S.; Wang, C.; Zhou, J.; Zeng, J.; Tan, W.; Wang, B. Effects of Nb Addition on the Properties and Microstructure of Cu-Ni-Si-Mg Alloy. *Mater. Charact.* **2022**, *194*, 112451. [[CrossRef](#)]
63. Güler, Ö.; Bağcı, N. A Short Review on Mechanical Properties of Graphene Reinforced Metal Matrix Composites. *J. Mater. Res. Technol.* **2020**, *9*, 6808–6833. [[CrossRef](#)]
64. Sharma, N.; Alam, S.N.; Ray, B.C. Fundamentals of Spark Plasma Sintering (SPS): An Ideal Processing Technique for Fabrication of Metal Matrix Nanocomposites. In *Spark Plasma Sintering of Materials*; Springer International Publishing: Cham, Switzerland, 2019; pp. 21–59.
65. Contreras Cuevas, A.; Bedolla Becerril, E.; Martínez, M.S.; Lemus Ruiz, J. Fabrication Processes for Metal Matrix Composites. In *Metal Matrix Composites*; Springer International Publishing: Cham, Switzerland, 2018; pp. 83–114.
66. Maca, K.; Pouchly, V.; Zalud, P. Two-Step Sintering of Oxide Ceramics with Various Crystal Structures. *J. Eur. Ceram. Soc.* **2010**, *30*, 583–589. [[CrossRef](#)]
67. Azimi, A.; Shokuhfar, A.; Zolriasatein, A. Nanostructured Al–Zn–Mg–Cu–Zr Alloy Prepared by Mechanical Alloying Followed by Hot Pressing. *Mater. Sci. Eng. A* **2014**, *595*, 124–130. [[CrossRef](#)]
68. Hidalgo-Manrique, P.; Lei, X.; Xu, R.; Zhou, M.; Kinloch, I.A.; Young, R.J. Copper/Graphene Composites: A Review. *J. Mater. Sci.* **2019**, *54*, 12236–12289. [[CrossRef](#)]
69. Makena, M.I.; Shongwe, M.B.; Ramakokovhu, M.M.; Olubambi, P.A. Effect of Sintering Parameters on Densification, Corrosion and Wear Behaviour of Ni-50Fe Alloy Prepared by Spark Plasma Sintering. *J. Alloys Compd.* **2017**, *699*, 1166–1179. [[CrossRef](#)]
70. Ercetin, A.; Pimenov, D.Y. Microstructure, Mechanical, and Corrosion Behavior of Al<sub>2</sub>O<sub>3</sub> Reinforced Mg<sub>2</sub>Zn Matrix Magnesium Composites. *Materials* **2021**, *14*, 4819. [[CrossRef](#)]
71. Xu, H.; Zou, N.; Li, Q. Effect of Ball Milling Time on Microstructure and Hardness of Porous Magnesium/Carbon Nanofiber Composites. *JOM* **2017**, *69*, 1236–1243. [[CrossRef](#)]
72. Wang, T.; Huang, Y.; Yang, L.; Ma, Y.; Wu, L.; Yan, H.; Liu, Y.; Liu, W. Preparation of 2024-Al/AZ31-Mg Laminated Composite by Powder Metallurgy Integrated Forming and Sintering. *JOM* **2020**, *72*, 3547–3557. [[CrossRef](#)]
73. Ercetin, A.; Özgün, Ö.; Aslantas, K. Investigation of Mechanical Properties of Mg5Sn-XZn Alloys Produced through New Method in Powder Metallurgy. *J. Test. Eval.* **2021**, *49*, 3506–3518. [[CrossRef](#)]
74. Nayyeri, G.; Mahmudi, R. Enhanced Creep Properties of a Cast Mg–5Sn Alloy Subjected to Aging-Treatment. *Mater. Sci. Eng. A* **2010**, *527*, 4613–4618. [[CrossRef](#)]
75. Özgün, Ö.; Aslantaş, K.; Erçetin, A. Powder Metallurgy Mg-Sn Alloys: Production and Characterization. *Sci. Iran.* **2020**, *27*, 1255–1265. [[CrossRef](#)]
76. Sadeghi, B.; Cavaliere, P.; Roen, G.A.; Nosko, M.; Shamanian, M.; Trembošová, V.; Nagy, Š.; Ebrahimzadeh, N. Hot Rolling of MWCNTs Reinforced Al Matrix Composites Produced via Spark Plasma Sintering. *Adv. Compos. Hybrid. Mater.* **2019**, *2*, 549–570. [[CrossRef](#)]
77. Romero, C.; Yang, F.; Bolzoni, L. Fatigue and Fracture Properties of Ti Alloys from Powder-Based Processes—A Review. *Int. J. Fatigue* **2018**, *117*, 407–419. [[CrossRef](#)]
78. Chen, H.; Mi, G.; Li, P.; Huang, X.; Cao, C. Microstructure and Tensile Properties of Graphene-Oxide-Reinforced High-Temperature Titanium-Alloy-Matrix Composites. *Materials* **2020**, *13*, 3358. [[CrossRef](#)]
79. Saba, F.; Sajjadi, S.A.; Heydari, S.; Haddad-Sabzevar, M.; Salehi, J.; Babayi, H. A Novel Approach to the Uniformly Distributed Carbon Nanotubes with Intact Structure in Aluminum Matrix Composite. *Adv. Compos. Hybrid. Mater.* **2019**, *2*, 540–548. [[CrossRef](#)]
80. Mokhtari, S.; Eftekhari Yekta, B.; Marghussian, V.; Ahmadi, P.T. Synthesis and Characterization of Biodegradable AZ31/Calcium Phosphate Glass Composites for Orthopedic Applications. *Adv. Compos. Hybrid. Mater.* **2020**, *3*, 390–401. [[CrossRef](#)]
81. Ma, J.; Li, Z.J.; Xue, Y.Z.B.; Liang, X.Y.; Tan, Z.J.; Tang, B. Novel PEEK/NHA Composites Fabricated by Hot-Pressing of 3D Braided PEEK Matrix. *Adv. Compos. Hybrid. Mater.* **2020**, *3*, 156–166. [[CrossRef](#)]

82. Suresh, S.; Gowd, G.H.; Kumar, M.L.S.D. Mechanical and Wear Behavior of Al 7075 / Al<sub>2</sub>O<sub>3</sub> / SiC / Mg Metal Matrix Nanocomposite by Liquid State Process. *Adv. Compos. Hybrid. Mater.* **2019**, *2*, 530–539. [[CrossRef](#)]
83. Xie, Y.; Meng, X.; Mao, D.; Qin, Z.; Wan, L.; Huang, Y. Homogeneously Dispersed Graphene Nanoplatelets as Long-Term Corrosion Inhibitors for Aluminum Matrix Composites. *ACS Appl. Mater. Interfaces* **2021**, *13*, 32161–32174. [[CrossRef](#)]

**Disclaimer/Publisher's Note:** The statements, opinions and data contained in all publications are solely those of the individual author(s) and contributor(s) and not of MDPI and/or the editor(s). MDPI and/or the editor(s) disclaim responsibility for any injury to people or property resulting from any ideas, methods, instructions or products referred to in the content.